










A Potential Second Shutoff from AT2018fyk: An Updated Orbital Ephemeris of the Surviving Star under the Repeating Partial Tidal Disruption Event Paradigm

Dheeraj Pasham¹ , E. R. Coughlin² , M. Guolo³ , T. Wevers⁴ , C. J. Nixon⁵ , Jason T. Hinkle^{6,7} , and A. Bandopadhyay² 

¹ MIT Kavli Institute for Astrophysics and Space Research Cambridge, MA 02139, USA

² Department of Physics, Syracuse University, Syracuse, NY 13210, USA

³ Department of Physics and Astronomy, Johns Hopkins University, 3400 N. Charles St., Baltimore MD 21218, USA

⁴ Space Telescope Science Institute, 3700 San Martin Drive, Baltimore, MD 21218, USA

⁵ School of Physics and Astronomy, Sir William Henry Bragg Building, Woodhouse Ln., University of Leeds, Leeds LS2 9JT, UK

⁶ Institute for Astronomy, University of Hawai'i at Manoa, 2680 Woodlawn Dr., Honolulu, HI 96822, USA

Received 2024 May 23; revised 2024 June 10; accepted 2024 June 10; published 2024 August 14

Abstract

The tidal disruption event (TDE) AT2018fyk showed a rapid dimming event 500 days after discovery, followed by a rebrightening roughly 700 days later. It has been hypothesized that this behavior results from a repeating partial TDE (rpTDE), such that prompt dimmings/shutoffs are coincident with the return of the star to pericenter and rebrightenings generated by the renewed supply of tidally stripped debris. This model predicted that the emission should shut off again around August of 2023. We report AT2018fyk's continued X-ray and UV monitoring, which shows an X-ray (UV) drop-in flux by a factor of 10 (5) over a span of two months, starting 2023 August 14. This sudden change can be interpreted as the second emission shutoff, which (1) strengthens the rpTDE scenario for AT2018fyk, (2) allows us to constrain the orbital period to a more precise value of 1306 ± 47 days, and (3) establishes that X-ray and UV/optical emission track the fallback rate onto this supermassive black hole—an often-made assumption that otherwise lacks observational verification—and therefore, the UV/optical lightcurve is powered predominantly by processes tied to X-rays. The second cutoff implies that another rebrightening should happen between 2025 May and August, and if the star survived the second encounter, a third shutoff is predicted to occur between 2027 January and July. Finally, low-level accretion from the less-bound debris tail (which is completely unbound/does not contribute to accretion in a nonrepeating TDE) can result in a faint X-ray plateau that could be detectable until the next rebrightening.

Unified Astronomy Thesaurus concepts: [Astrophysical black holes \(98\)](#); [Supermassive black holes \(1663\)](#); [Tidal disruption \(1696\)](#); [X-ray astronomy \(1810\)](#); [Ultraviolet astronomy \(1736\)](#); [Transient sources \(1851\)](#); [Time domain astronomy \(2109\)](#)

1. Introduction

A tidal disruption event (TDE) occurs when a star approaches a supermassive black hole (SMBH) and is either completely or partially destroyed (e.g., Rees 1988; Gezari 2021). TDE candidates were first discovered in the mid 1990s in the X-rays using the ROSAT soft X-ray telescope (XRT; e.g., Grupe et al. 1995; Bade et al. 1996; Donley et al. 2002) and more recently with optical sky surveys like the ASASSN (Shappee et al. 2014), ATLAS (Tonry et al. 2018), Zwicky Transient Facility (ZTF; Bellm 2019), and with eROSITA in the X-rays (Sazonov et al. 2021). With an estimated observed rate of roughly one TDE every 10^{4-5} yr per galaxy (Sazonov et al. 2021; Yao et al. 2023), there is huge excitement for Rubin observatory (first light in 2024), which is expected to identify >100 events every year (van Velzen et al. 2011; Bricman & Gomboc 2020).

A few dozens of TDEs are known so far, and they have already transformed our understanding of SMBHs and their immediate surroundings. For example, some TDEs that were followed up extensively in the X-rays have shown powerful

outflows (e.g., see Kara et al. 2018; Kosec et al. 2023; Ajay et al. 2024; Wevers et al. 2024). Some systems have highly relativistic jets (bulk Lorentz factor \sim a few tens) akin to blazars and have provided the best data sets to test models of jet launching (e.g., see Bloom et al. 2011; Brown et al. 2015; Pasham et al. 2015; Andreoni et al. 2022; Pasham et al. 2023; Yao et al. 2024). In a few systems, radio synchrotron expanding at subrelativistic speeds has been found, which can be either from internal shocks within a jet (Pasham & van Velzen 2018) or from external shocks with ambient medium (Cendes et al. 2023).

In addition to these TDE subclasses, in the last few years, a surprising new subclass has been uncovered: those that repeat on timescale of months to years (Payne et al. 2021, 2022; Liu et al. 2023b; Evans et al. 2023; Payne et al. 2023; Somalwar et al. 2023; Wevers et al. 2023; Guolo et al. 2024; Lin et al. 2024). These events have been postulated to arise from a star on a bound orbit about an SMBH that is partially disrupted during each pericenter passage. The TDE AT2018fyk/ASASSN-18ul (redshift $z = 0.059$, luminosity distance of 264.3 Mpc) is thought to be one example of this new class and was discovered by the ASAS-SN optical survey in 2018, and follow-up monitoring with Swift, NICER, XMM-Newton, and Chandra showed that it remained X-ray and UV bright for roughly 500 days. Thereafter, it displayed a sudden and dramatic decrease in the X-ray (by a factor of >6000) and the UV (by a factor of ≈ 15 ; see Figure 2 and Wevers et al. 2021). The source also exhibited apparent

⁷ NASA FINESST FL.

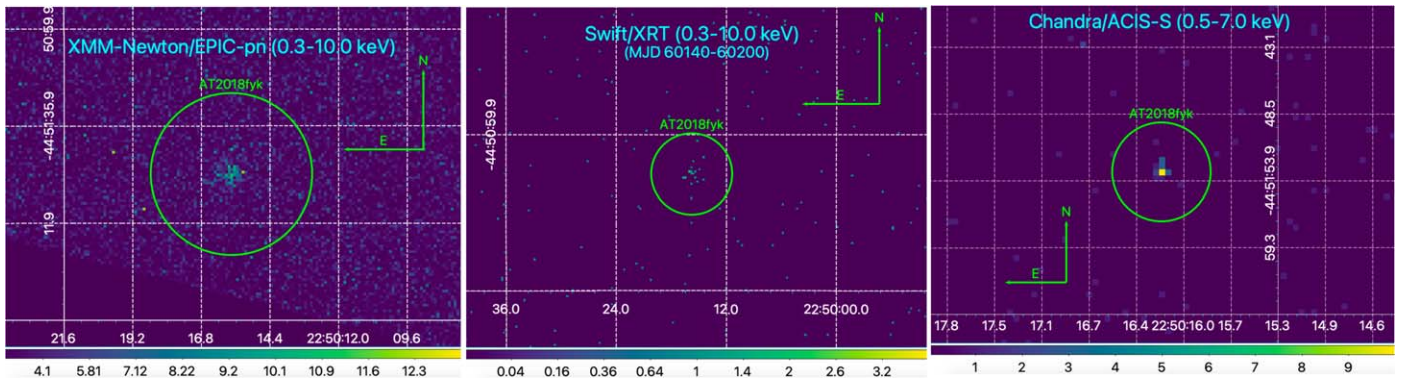


Figure 1. Left: XMM-Newton/EPIC-pn image of AT2018fyk’s field of view on MJD 60102.76 (XMM ObsID 0921510101). The circle centered on AT2018fyk has a radius of $30''$, while the arrows pointing north and east are each $30''$ in length. Middle: stacked Swift/XRT image of AT2018fyk using data taken between MJDs 60140 and 60200, i.e., the data point around day 1800 between XMM-Newton (pentagon) and Chandra detections (square) in Figure 2. The statistical significance of the detection is 3.7σ . The circle has a radius of $47''$, while the directional arrows are $90''$ each. Right: stacked Chandra/ACIS X-ray image using data from ObsIDs 28294 and 28972. The circle centered on AT2018fyk has a $4''$ radius while the directional arrows are $5''$ each.

state transitions similar to outbursting stellar-mass black hole binaries (soft/UV/accretion disk dominated state \Rightarrow hard/X-ray/corona-dominated state \Rightarrow quiescence; see Wevers et al. 2021).

The source was then found to be X-ray and UV bright again around day ~ 1200 ,⁸ with eROSITA nondetections interspersed between the last nondetection at day 600 and the first new detection at day 1200, showing that AT2018fyk suddenly “turned on” following a ~ 2 yr dark period—behavior that is otherwise unprecedented in observed TDEs. The precipitous drop in luminosity and the rebrightening can be explained by the rpTDE scenario:⁹ Wevers et al. (2023) argued that if the return of the tidally disrupted debris to the SMBH is tightly coupled to the accretion rate and the corresponding luminosity, which is a good approximation for highly relativistic settings with small viscous delays, the sudden cessation of accretion coincides with the return of the star to pericenter, and the time between the sudden cutoff and the rebrightening equates to the fallback time of the tidally stripped debris. With this model, they deduced that the orbital period of the star is ~ 1200 days. They predicted that, if the star was not destroyed during the second pericenter passage, the system should display another dimming in 2023 August, analogous to the one observed in 2019.

Here, using continued X-ray monitoring with Swift, NICER, XMM-Newton, and Chandra, we report the finding of this second cutoff at 1830 ± 29 days (2023 August 14–October 11). Our data analysis is shown in Section 2 while we discuss the implications and provide specific predictions to further test the rpTDE model in Section 3.

2. Data and Analysis

We used the following cosmological parameters: Λ CDM cosmology with parameters $H_0 = 67.4 \text{ km s}^{-1} \text{ Mpc}^{-1}$, $\Omega_m = 0.315$, and $\Omega_\Lambda = 1 - \Omega_m = 0.685$ (Planck Collaboration et al. 2020).

⁸ All times in this Letter are measured in the observer’s frame with respect to the optical discovery date of MJD 58369.2.

⁹ The presence of an active galactic nucleus in AT2018fyk was ruled out based on detailed analyses of multiwavelength data of the host galaxy; see Section 2.4 of Wevers et al. (2023).

2.1. Swift X-Ray Data

Swift (Gehrels et al. 2004) observed AT2018fyk on 210 occasions as of 2024 January 5. Out of these, five were corrupted or did not have photon counting data and were excluded. Observations up to MJD 59809, i.e., 178 of these observations, were reported in Wevers et al. (2023). Here we present additional monitoring data since 2022 August 18. For consistency, we reduce the entire Swift archival data of AT2018fyk here.

We started our analysis by downloading the data from HEASARC public archive¹⁰ and reduced the XRT (Burrows et al. 2005) observations on a per ObsID basis using the HEASoft tool `xrtpipeline`. Then we extracted source and background count rates in the 0.3–10.0 keV band using the `ftool xrtlccorr`. We used a circular aperture of radius $47''$ for source and an annulus of inner and outer radii of $70''$ and $235''$, respectively. These values were chosen to ensure there are no contaminating sources within the chosen boundaries. From these, we obtained a net (background-subtracted) rate for each ObsID.

AT2018fyk was especially faint with net rates close to zero in the most recent observing campaign since MJD 60000 (approved Swift cycle 19 program 1922148; PI: Pasham). Therefore, we carefully analyzed them by stacking them into four data sets with the following time boundaries: MJD 60030–60070 (L1), MJD 60070–60140 (L2), MJD 60140–60200 (L3), and MJD 60200–60310 (L4). The source was detected in two of these four stacked data sets. The net 0.3–10.0 keV count rate/ 3σ upper limit for L1, L2, L3, and L4 epochs were $(1.5 \pm 0.6) \times 10^{-3}$ cps, $< 4.3 \times 10^{-3}$ cps, $(2.6 \pm 0.7) \times 10^{-3}$ cps, and $< 2 \times 10^{-3}$ cps, respectively. We also visually inspected the exposure-corrected 0.3–10.0 keV image for epoch L3 in which a point source is evident (see the middle panel of Figure 1). Assuming a spectrum similar to the one implied by an XMM-Newton observation taken around that time, the flux conversion factor is $3.1 \times 10^{-11} \text{ erg s}^{-1} \text{ cm}^{-2} \text{ counts}^{-1} \text{ sec}$.

2.2. Swift UV Data

UV observations were taken with Swift/UVOT contemporaneously with the XRT observations. We used the `uvot-source` package to measure the UV photometry, using an

¹⁰ <https://heasarc.gsfc.nasa.gov/cgi-bin/W3Browse/w3browse.pl>

aperture of $5''$. We subtracted the host galaxy contribution by modeling archival photometry data with stellar population synthesis using PROSPECTOR (Johnson et al. 2021), following the procedure described in Wevers et al. (2021) and tabulated in their Table 2. We apply Galactic extinction correction to all bands using the $E(B - V)$ value of 0.011 from Schlafly & Finkbeiner (2011).

2.3. XMM-Newton

XMM-Newton observed AT2018fyk on eight occasions (ObsIDs: 0831790201, 0853980201, 0854591401, 0911790701, 0911790601, 0911791501, 0911791401, and 0921510101). Two observations (0911790701 and 0911791501) did not have any science data, and the rest, except for the latest one (ObsID: 0921510101), have been published elsewhere (Wevers et al. 2019, 2021, 2023). This latest data set was part of an approved XMM-Newton Cycle 22 Guest Observer Target of Opportunity (program 92151; PI: Pasham) to capture the second X-ray shutoff of AT2018fyk. While the main focus in this work will be on this latest data set, we also reduce all the others here for uniformity.

We started XMM-Newton data analysis by downloading the data from the HEASARC public archive.¹¹ Then we ran the `epproc` tool of XMMSAS software to reduce the European Photon Imaging Camera (EPIC)'s pn detector. We did not use MOS data in this work. First, we visually inspected the background in all the six ObsIDs following the steps outlined in the data analysis thread: <https://www.cosmos.esa.int/web/xmm-newton/sas-thread-epic-filterbackground-in-python>. All observations were affected by background flares to some extent, and we removed those epochs to obtain a set of good time intervals per ObsID. Source events were extracted from a circular aperture with a radius of $30''$, while background events were extracted from a nearby circular aperture free of any point sources with a radius of $50''$. The source is clearly detected in all but 0854591401 (XMM3 as per Wevers et al. 2023). Consequently, five spectra were extracted following the standard procedure outlined here: <https://www.cosmos.esa.int/web/xmm-newton/sas-thread-pn-spectrum>. The spectra were grouped using the `specgroup` task of XMM-Newton software (XMMSAS) to have minimum of 1 count per spectral bin. Cash statistic was used for spectral modeling in XSPEC (Arnaud 1996). For each spectrum, we only used the bandpass where the source is above the background (see Table 1).

The most recent data set is consistent with a simple power law modified by Milky Way absorption of $1.2 \times 10^{20} \text{ cm}^{-2}$ (C-stat/degrees of freedom, dof, of 110/114). Additional absorption at the host redshift is not required by the data in any of the five spectra. The best-fit power-law index in the most recent data set is $1.96_{-0.88}^{+0.86}$ (see Table 1 for details on flux and luminosity). The spectrum did not have enough signal-to-noise to test more complicated spectral models.

2.4. Chandra

Chandra's Advanced CCD Imaging Spectrometer (ACIS) observed AT2018fyk on three occasions: MJD 59029.22 (2020 June 29), MJD 60227.71 (2023 October 10; ObsID: 28294), and MJD 60228.58 (2023 October 11; ObsID: 28972). All these were carried out in the ACIS-S array mode, and we use the nominal bandpass of 0.5–7.0 keV throughout. The first

observation was published in Wevers et al. (2021), while the most recent two data sets were observed as part of an approved Chandra Cycle 25 guest observer program to catch the source during the second shutoff phase predicted by Wevers et al. (2023; PI: Pasham; Guest Observer proposal number 25700383). For consistency, we reduce all the three data sets here.

We started our data analysis by reducing the data with the `chandra_repro` tool of CIAO 4.16 software using the latest CALDB 4.11.0. First, we extracted exposure-corrected images in the 0.5–7.0 keV bandpass using the `fluximage` task of CIAO and see an excess at the position of AT2018fyk in both of the most recent observations (IDs: 28294 and 28972). Next, we extracted the X-ray spectra and relevant response files for each of the two recent observations separately using `specextract` tool of CIAO. These spectra were grouped to have a minimum of one spectral count per bin using the `optmin` flag of the HEASoft `ftol` `ftgroup` task. We modeled them together in XSPEC (Arnaud 1996) with a power-law model modified by Milky Way neutral absorption column of $1.2 \times 10^{20} \text{ cm}^{-2}$ (*tbabs*zabs*powerlaw*). With only 25 net (background-corrected) counts, the spectral index is poorly constrained. Therefore, we fixed it at the best-fit value from the XMM-Newton data of 1.96. This yields a best-fit C-statistic/dof of 38.5/56 and an observed 0.3–10.0 keV flux (luminosity) of $(9.0_{-2.0}^{+1.0}) \times 10^{-15} \text{ erg s}^{-1} \text{ cm}^{-2}$ ($(7.0_{-1.0}^{+2.0}) \times 10^{40} \text{ erg s}^{-1}$). This represents a factor of >7 decrease in flux since the latest XMM-Newton observation taken roughly four months earlier.

2.4.1. Chandra Astrometry

We also combined the two observations to estimate an accurate position by following the steps outlined in https://cxc.cfa.harvard.edu/ciao/threads/fluxes_multiobi/. We computed the offsets between the two data sets to be 0.18 pixels and 0.42 pixels in the X- and Y-directions, respectively. To improve this, we performed astrometric correction to obsID 28972 to match with that of 28294, which has about 60% higher exposure time (33 ks versus 20 ks). Following the steps outlined in the above Chandra data analysis thread, we reduced the offsets to 0.15 pixels and 0.06 pixels, respectively. An X-ray (0.5–7.0 keV) image from combining obsIDs 28294 and 28972 is shown in the right panel of Figure 1. The source region defined as a circular aperture of $4''$ in radius has 25 net counts. Running `wavdetect` on this combined images yields a best-fit X-ray position of (22:50:16.17, $-44:51:53.00$) with an uncertainty of $0''.12$ in each direction. This is consistent with the best-fit Gaia position reported in Wevers et al. (2019) based on the optical emission during the first outburst in 2018.

2.5. Hubble Space Telescope

The UV measurement from Hubble Space Telescope's F275W filter with an effective wavelength of 2750 Å was taken from Wen et al. (2024).

2.6. Shutoff and Rebrightening Times

The first X-ray and UV shutoffs happened between days 488 and 561, while the second sharp decline occurred sometime during days 1801 and 1859 (see Figure 2). These values correspond to the observation dates. Per the model of Wevers et al. (2023), the orbital period of the surviving star is the time

¹¹ <https://heasarc.gsfc.nasa.gov/cgi-bin/W3Browse/w3browse.pl>

Table 1
Summary of XMM-Newton and Chandra X-ray Energy Spectral Modeling

Telescope	ObsID	MJD	Exposure ^a (ks)	Count Rate ^b (counts sec ⁻¹)	Bandpass ^c (keV)	kT (keV)	N_{kT} ^d	Γ ^e	N_{Γ} ^f ($\times 10^{-5}$)	Flux ^g $\times 10^{-13}$ (erg s ⁻¹ cm ⁻²)	Luminosity ^g (10^{42} erg s ⁻¹)	C-stat/dof
XMM	0831790201	58461.72	17.0 (33)	0.403 ± 0.004	0.3–2.5	$0.123^{+0.005}_{-0.004}$	493^{+100}_{-164}	$3.41^{+0.68}_{-1.38}$	$3.4^{+1.4}_{-1.9}$	$7.7^{+0.2}_{-0.1}$	$7.0^{+0.3}_{-0.1}$	42.4/48
XMM	0853980201	58783.33	35.0 (55)	0.687 ± 0.004	0.3–9.0	$0.146^{+0.006}_{-0.006}$	170^{+32}_{-25}	$2.07^{+0.06}_{-0.06}$	$22.6^{+1.4}_{-1.4}$	$15.7^{+0.1}_{-0.2}$	$13.3^{+0.1}_{-0.2}$	192.0/155
XMM	0911790601	59719.89	8.2 (29)	0.175 ± 0.005	0.3–5.0	$0.095^{+0.035}_{-0.032}$	211^{+1700}_{-173}	$2.35^{+0.19}_{-0.22}$	$8.6^{+0.8}_{-1.1}$	$3.7^{+0.3}_{-0.3}$	$3.2^{+0.3}_{-0.3}$	72.1/82
XMM	0911791401	59739.84	3.1 (10.6)	0.130 ± 0.009	0.3–0.8	$2.77^{+0.54}_{-0.54}$	$11.1^{+4.4}_{-3.4}$	$4.4^{+1.4}_{-0.6}$	$3.7^{+0.8}_{-0.6}$	15.0/11
XMM	0921510101	60102.76	8.8 (43.1)	0.011 ± 0.001	0.3–1.0	$1.96^{+0.86}_{-0.88}$	$1.1^{+0.6}_{-0.4}$	$0.6^{+0.7}_{-0.2}$	$0.5^{+0.3}_{-0.2}$	19.1/16
Chandra ^h	28294	60227.71	32.6 (33)	$(3.8 \pm 1.2) \times 10^{-4}$	0.5–7.0	1.96	$0.18^{+0.08}_{-0.06}$	$0.09^{+0.01}_{-0.02}$	$0.07^{+0.02}_{-0.01}$	38.5/56
Chandra ^h	28972	60228.58	19.8 (20)	$(5.0 \pm 1.7) \times 10^{-4}$	0.5–7.0	1.96	$0.18^{+0.08}_{-0.06}$	$0.09^{+0.01}_{-0.02}$	$0.07^{+0.02}_{-0.01}$	38.5/56

Notes.

^a The net exposure after filtering for background flares. Total exposure before correcting for flares is shown in parentheses.

^b Net count rate (background-corrected) in the bandpass where the source is above the background.

^c Bandpass where the source and the background spectrum cross over. This is different for each spectrum, and modeling was performed in this custom band depending on the observation. We repeated the entire analysis in a fixed 0.3–1.5 keV band, and the resulting values were consistent with those reported in this table.

^d Normalization of the best-fit disk blackbody.

^e Power-law index.

^f Normalization value of the power-law model component.

^g Observed flux and luminosities in the 0.3–10.0 keV band. *tbabs*zashift(diskbb+pow)* was used for modeling. In cases where kT is indicated by an ellipsis, a disk component was not necessary.

^h Both the Chandra spectra were fit together, hence the same spectral parameters. The power-law index was fixed at the best-fit XMM-Newton value from ObsID 0921510101.

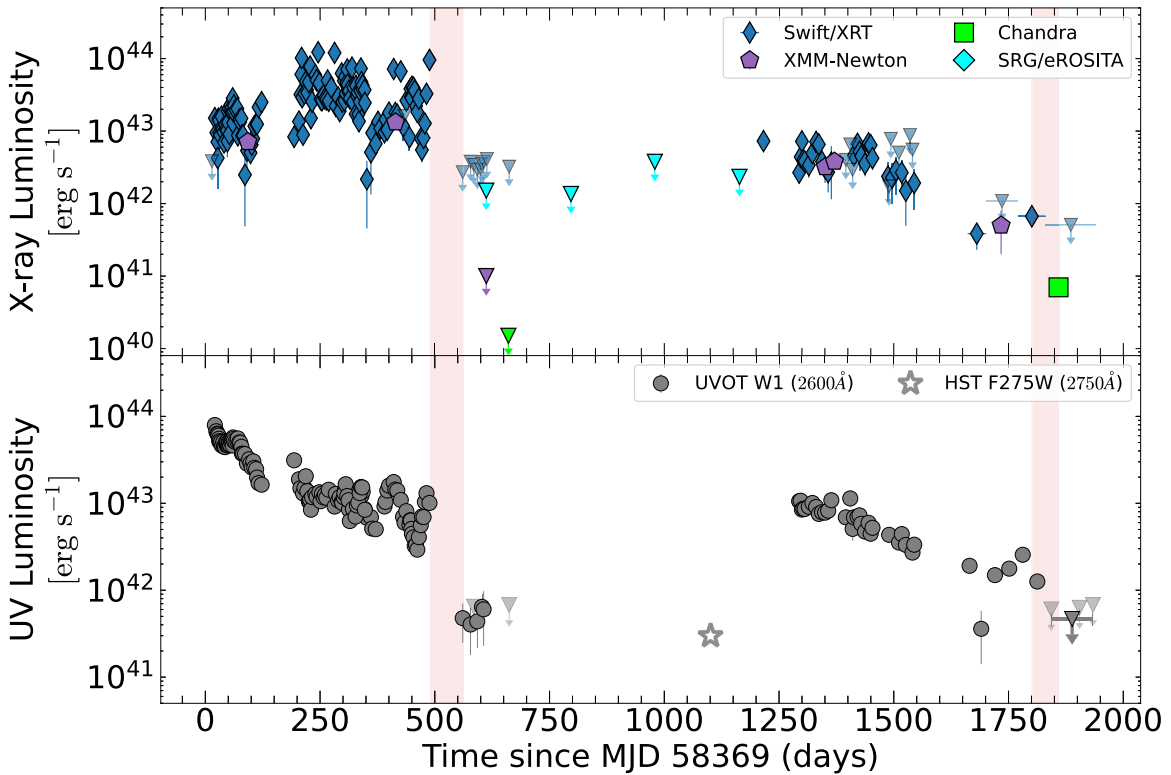


Figure 2. Top: AT2018fyk’s observed 0.3–10.0 keV X-ray luminosity evolution over the past ~ 2000 days. The x-axis is in the observer’s frame. Most recent Chandra and Swift data show a drop of >10 from 7×10^{42} to 7×10^{41} over two months. A similar change is also evident in the UV lightcurve (bottom panel). Inverted triangles represent 3σ upper limits. This sudden change can be interpreted as a shutoff, which allows us to refine the orbital period of the star that is repeatedly disrupted to be 1306 ± 47 days. The two shutoff epochs are highlighted with red/vertical bands. The entire X-ray and UV photometry is available at doi:[10.5281/zenodo.10913475](https://doi.org/10.5281/zenodo.10913475).

between shutoffs, which, based on the above values, is 1306 ± 47 days.¹² The uncertainty is derived from adding the range in cutoff times in quadrature. Using this, we can formulate a crude ephemeris to predict the n th shutoff to be

$$t_{\text{shutoff}}^n (\text{MJD}) = (58893.5 \pm 29) + (n - 1)(1306 \pm 47).$$

This equation implies that the next (third) shutoff should occur sometime between 2027 January 2 and 2027 July 17, assuming that the star survived its second encounter. Alternatively, if the star was completely destroyed during the second encounter, then there would be no third cutoff, and the luminosity would continue to smoothly decline.¹³

The fallback time after the second pericenter passage of the star is the time between the first shutoff and the second rebrightening (between 1164 and 1216 days). The fallback time will differ from one encounter to the next because mass is stripped from the progenitor and the star is imparted a net rotation (Bandopadhyay et al. 2024a), and hence accurately predicting the next rise is not as straightforward as predicting the orbital period. However, if we assume a similar fallback time, then the next rise in flux should happen around

2495 ± 54 days, which corresponds to an MJD 60864 ± 54 (2025 May 15–2025 August 31).

The latest Chandra data point (green square in Figure 2) is 2 orders of magnitude below the peak of the second outburst and an order of magnitude below a previous XRT detection roughly two months earlier. However, it is possible that the latest Chandra data and the corresponding UV upper limits may be due to anomalous source variability. For this reason, we refer to this as a potential shutoff. This can be confirmed with further deep X-ray and UV observations between now and the predicted next rebrightening in 2025.

3. Discussion and Conclusions

The rpTDE model proposes that a star is on a highly eccentric ($0.99 \lesssim e < 1$) orbit about an SMBH, with the short orbital period and high eccentricity provided by the Hills mechanism (Cufari et al. 2022; Wevers et al. 2023). Since the fallback time inferred from the observations is ~ 600 – 700 days, the SMBH powering the emission from AT2018fyk must be large and the disruption must be partial, as both of these effects increase the return time of the debris above the $\sim (30 \pm 5) \times (M./10^6 M_{\odot})^{1/2}$ days that is characteristic of complete disruptions, with $M.$ the SMBH mass (Coughlin & Nixon 2022; Bandopadhyay et al. 2024b).

When the SMBH mass is large (as is inferred to be the case for AT2018fyk; $10^{7.7 \pm 0.4}$; see Wevers et al. 2023), the accretion rate should be strongly coupled to the fallback rate of debris because the pericenter distance is highly relativistic and the accretion timescale is short relative to the fallback time. This model then predicts that the accretion rate should shut off

¹² Note that Wevers et al. (2023) estimated the orbital period of the star by assuming that the fallback time between the first and second encounters was the same, and while this is likely a fairly good approximation, observing the successive shutoffs is more direct. See Section 3 for additional discussion.

¹³ We note that this possibility may provide a unique opportunity to explore the differences in emission produced by fallback from partial and complete disruption events in the same system, i.e., comprising the same black hole mass and spin and stellar orbit.

when the surviving core returns to the (partial) tidal disruption radius (Wevers et al. 2023; see also Liu et al. 2023a), the reason being that the Hill sphere that separates material bound to the black hole and bound to the star grows with time approximately as $\propto t^{2/3}$, where t is time since pericenter (Coughlin & Nixon 2019). Therefore, when the surviving core returns to pericenter, there is a sudden drop in the mass supply to the SMBH, and the luminosity plummets. The simultaneous plummeting of the optical/UV emission alongside the X-ray is also consistent with the interpretation that the optical/UV emission is tied to X-ray emission¹⁴ that originates from the innermost few gravitational radii, which in this case may be physically produced by circularization shocks, accretion, or both (the former may also give rise to the nonthermal electrons powering the corona; see Sironi & Tran 2024).

The time between successive cutoffs in emission should therefore closely track the orbital period of the stellar core. Because the orbital period is related to the orbital energy and the orbital energy can at most be reduced by the binding energy of the star, there is effectively no change in this recurrence time on a per-orbit basis (Cufari et al. 2023; Bandopadhyay et al. 2024a).¹⁵ On the other hand, the time between the cutoff and the next rebrightening equals the fallback time of the most-bound debris that is related to the properties of the star and its rotation rate, and the latter changes as a consequence of the tidal interaction with the SMBH (since the imparted spin is prograde with respect to the orbital angular momentum, the result is a decrease in the return time of the debris; Golightly et al. 2019). Wevers et al. (2023) estimated the orbital time of the star—and thereby predicted the time of the second cutoff—by assuming that the fallback time was unchanged between the first and second encounters: since the first cutoff occurred at ~ 500 days (since the first detection) and the second brightening at ~ 1200 days, the fallback time (for the second encounter) was ~ 700 days, and the first pericenter passage must have occurred ~ 700 days prior to the first detection if the fallback times were identical on the first and second encounters, making the orbital period of the star ~ 1200 days. If we now associate the green data point at day ~ 1850 as the second observed cutoff (note that this date also coincides with the observed cutoff in the optical/UV, which is qualitatively in agreement with the behavior observed during the first cutoff), then this suggests that the true (i.e., from the observed successive cutoffs) orbital period of the star is between 1250 and 1350 days. This finding suggests that the fallback time on the second encounter was shorter than that of the first by ~ 50 – 150 days, which is different at the $\sim 10\%$ – 20% level. This is consistent with the theoretical results of Golightly et al. (2019) if the imparted spin to the star was a significant fraction of the breakup (which is expected, given the importance of nonlinear interactions when

the tidal field of the SMBH is comparable to the self-gravitational field of the star). If the star is spun up to a closer fraction of the angular velocity at pericenter on its third encounter, we would expect a reduced fallback time in going from the second shutoff to the start of the third electromagnetic outburst, and the observation (or lack thereof) of this feature would provide another test of this model.

A noticeable difference between the first and second outbursts in AT2018fyk’s lightcurve is the peak luminosity, which is reduced by a factor of ~ 5 – 10 from the first to second brightenings. Under the rpTDE paradigm, this difference could be due to one or more potential factors. If, for example, the partially disrupted star was highly centrally concentrated—which would arise naturally as a consequence of stellar evolution if the star is sufficiently massive—then it seems plausible that the stripping of the envelope on the first encounter could leave the high-density core relatively unperturbed, the result being that the tidal radius of the surviving core is smaller. Since the pericenter distance of the star is effectively unaltered owing to the conservation of angular momentum, the $\beta (=r_t/r_p)$, with r_p the pericenter distance and r_t the tidal radius) of the encounter is reduced, resulting in less mass stripped on subsequent tidal interactions and a reduction in the accretion rate (and the luminosity).

Bandopadhyay et al. (2024a) recently showed (and in agreement with the suggestion by Liu et al. 2023a) that more massive and evolved stars (specifically a $1.3 M_\odot$ and a $3 M_\odot$ star near the end of the main sequence) that require very deep encounters to be completely destroyed—and are thus statistically significantly more likely to be partially disrupted—are capable of producing flares of nearly equal amplitude after many successive outbursts, despite the fact that the amount of mass stripped from the star declines slightly per pericenter passage (see their Figures 7, 8, and 11). Contrarily, a Sun-like star closer to the zero-age main sequence, which is significantly less centrally concentrated than an evolved star of the same mass, was shown by the same authors to suffer increasing degrees of mass loss per encounter, even when the pericenter distance of the encounter was a factor of ~ 3 larger than that required to completely destroy the star on the first encounter (see their Figure 13; see also Liu et al. 2024, who came to similar conclusions regarding the fate of a solar-like star after multiple encounters). Similarly, since a star of significantly lower mass ($\lesssim 0.1 \times \text{few } M_\odot$) cannot evolve substantially over the age of the Universe and is effectively a $5/3$ polytrope, the range in radii where such a low-mass star could be repeatedly stripped of a small amount of mass $\beta \simeq 0.5 - 0.6$ (Guillochon & Ramirez-Ruiz 2013; Mainetti et al. 2017; Miles et al. 2020; Cufari et al. 2023) per encounter is very finely tuned, and the detection of a second cutoff here suggests that the star must have survived at least two encounters. Thus, and despite their relative rarity, a more massive star could be the most promising candidate for producing the repeated flares in 2018fyk. A more massive star would also permit wider initial binaries (while yielding the same period of the captured star), a less relativistic pericenter distance, and a longer fallback time of the tidally stripped debris compared to the more extreme values required for a solar-like star to fit the observations (see the discussion in Section 4 of Wevers et al. 2023).

Additionally, if the Hills mechanism is responsible for placing the star on its tightly bound orbit about the SMBH, then there will be a difference between the pericenter distance

¹⁴ This seems inconsistent with the interpretation that the optical/UV is sourced from a large-scale outflow that is causally disconnected from the X-ray emission (e.g., Price et al. 2024).

¹⁵ This holds for orbits generated by the Hills disruption of a tight binary, where by tight we mean that the binding energy of the binary is comparable to the binding energy of the captured star (which was one of the members of the original binary). In this case, the binding energy of the captured star’s orbit is larger than that of the star itself by a factor of $(M_c/M_*)^{1/3}$ (e.g., Cufari et al. 2022). On the other hand, for a standard TDE in which the binding energy of the star’s orbit is ~ 0 , the change in the energy of the core during core reformation (e.g., Nixon et al. 2021; Nixon & Coughlin 2022) or due to a positive-energy kick (e.g., Manukian et al. 2013; Gafton et al. 2015) can give rise to substantial differences in the orbital period between successive partial disruptions.

of the partially disrupted (and captured) star during its initial hydrodynamical interaction between the SMBH and the (ultimately ejected) companion star and subsequent encounters. If it is such that the roughly conserved pericenter distance of the captured star is larger than that of the initial interaction, then less mass will be stripped on the second encounter, resulting in a relatively smaller accretion luminosity on the second outburst. Depending on how centrally concentrated the star is and the β of the encounter, subsequent outbursts could be progressively more or less luminous with time. As also discussed in Bandopadhyay et al. (2024a), the tight binary required to populate the star on its ~ 1300 day orbit implies that the rotation rate of the captured star is a significant fraction of the angular velocity at pericenter, which will also have a significant impact on the magnitude of successive flares and the return time of the debris (Golightly et al. 2019).

From the rpTDE model, the orbital time of the star is ~ 1200 – 1400 days, and the fallback time is ~ 600 – 800 days (note that such long fallback times require the event to be a partial disruption; Bandopadhyay et al. 2024a), which predicts that the freshly stripped debris generated on the third encounter (i.e., the second dimming around the green point in Figure 2) should produce a third brightening at day ~ 2500 post-initial detection (though, as noted above, the additional imparted spin to the star near pericenter could yield a time closer to day ~ 2400). This third brightening should then occur in early 2025, which is consistent with the predictions in Wevers et al. (2023), and the future detection or nondetection thereof would provide strong evidence in support of or against this model.

An alternative interpretation, as proposed by Wen et al. (2024), is that the reduction in the luminosity of AT2018fyk is due to the presence of a companion black hole and that the disrupting black hole was of very low mass compared to the primary. In such extreme-mass-ratio systems, there could be a dramatic dimming when the tidally stripped debris nears the Hill sphere of the secondary (disrupting) black hole after the first encounter, provided that the orientation of the binary is favorable (Coughlin & Armitage 2018). Wen et al. (2024) then proposed that the second outburst arose from accretion onto the primary. However, when the secondary is the disrupting SMBH, and the stream is relatively confined to the orbital plane of the binary—which must be the case if accretion onto the primary is responsible for the second outburst—the distribution of the debris is highly stochastic (see, e.g., Figures 1 and 2 of Coughlin & Armitage 2018 or Figures 9 and 10 of Coughlin et al. 2017), and it is difficult to see why this scenario would produce repeated and dramatic dimmings on this same timescale.

Finally, the partial TDE results in the production of two tails of stellar debris. In typical TDEs where the star is on a parabolic orbit, the second tail is ejected from the system and yields no observational signature (with the possible exception of radio emission in the presence of circumnuclear gas; e.g., Guillochon et al. 2016; Yalinewich et al. 2019). However, and as noted in Wevers et al. (2023), the bound nature of the stellar orbit in this case implies that the second tail may be “less bound” rather than unbound, with the specific energy of the second tail a function of the specific energy of the core and the energy spread imparted by the tidal field. It could be that deeper X-ray monitoring of AT2018fyk during the second (current) shutoff phase would reveal the presence of low-level emission from this second tail, and since the energy of the core is constrained from the observed orbital period, this emission






would yield additional information about the properties of the star and the SMBH. rpTDEs are thus unique in their ability to more directly constrain stellar and SMBH properties in distant galaxies.

Acknowledgments

D.R.P. was supported by NASA XMM-Newton guest observer program, proposal number 92395 (award number 035212-00001), and Chandra program 25700383 (award number 035385-00001). E.R.C. and A.B. acknowledge support from NASA through the *Neil Gehrels* Swift Guest Investigator Program, proposal number 1922148. E.R.C. acknowledges additional support from the National Science Foundation through grant AST-2006684 and from NASA through the Astrophysics Theory Program, grant 80NSSC24K0897. C.J.N. acknowledges support from the Science and Technology Facilities Council (grant No. ST/Y000544/1) and from the Leverhulme Trust (grant No. RPG-2021-380). This research was supported in part by grant NSF PHY-2309135 to the Kavli Institute for Theoretical Physics (KITP).

This Letter employs a list of Chandra data sets, obtained by the Chandra X-ray Observatory, contained in doi:10.25574/cdc.255.

ORCID iDs

Dheeraj Pasham  <https://orcid.org/0000-0003-1386-7861>
 E. R. Coughlin  <https://orcid.org/0000-0003-3765-6401>
 M. Guolo  <https://orcid.org/0000-0002-5063-0751>
 T. Wevers  <https://orcid.org/0000-0002-4043-9400>
 C. J. Nixon  <https://orcid.org/0000-0002-2137-4146>
 Jason T. Hinkle  <https://orcid.org/0000-0001-9668-2920>
 A. Bandopadhyay  <https://orcid.org/0000-0002-5116-844X>

References

- Ajay, Y., Pasham, D. R., Wevers, T., et al. 2024, arXiv:2401.12908
 Andreoni, I., Coughlin, M. W., Perley, D. A., et al. 2022, *Natur*, 612, 430
 Arnaud, K. A. 1996, in ASP Conf. Ser. 101, *Astronomical Data Analysis Software and Systems V*, ed. G. H. Jacoby & J. Barnes (San Francisco, CA: ASP), 17
 Bade, N., Komossa, S., & Dahlem, M. 1996, *A&A*, 309, L35
 Bandopadhyay, A., Coughlin, E. R., Nixon, C. J., & Pasham, D. R. 2024a, arXiv:2406.03675
 Bandopadhyay, A., Fancher, J., Athian, A., et al. 2024b, *ApJL*, 961, L2
 Bellm, E., Kulkarni, S. R., Graham, M. J., et al. 2019, *PASP*, 131, 018002
 Bloom, J. S., Giannios, D., Metzger, B. D., et al. 2011, *Sci*, 333, 203
 Bricman, K., & Gomboc, A. 2020, *ApJ*, 890, 73
 Brown, G. C., Levan, A. J., Stanway, E. R., et al. 2015, *MNRAS*, 452, 4297
 Burrows, D. N., Hill, J. E., Nousek, J. A., et al. 2005, *SSRv*, 120, 165
 Cendes, Y., Berger, E., Alexander, K. D., et al. 2023, arXiv:2308.13595
 Coughlin, E. R., & Armitage, P. J. 2018, *MNRAS*, 474, 3857
 Coughlin, E. R., Armitage, P. J., Nixon, C., & Begelman, M. C. 2017, *MNRAS*, 465, 3840
 Coughlin, E. R., & Nixon, C. J. 2019, *ApJL*, 883, L17
 Coughlin, E. R., & Nixon, C. J. 2022, *MNRAS*, 517, L26
 Cufari, M., Coughlin, E. R., & Nixon, C. J. 2022, *ApJL*, 929, L20
 Cufari, M., Nixon, C. J., & Coughlin, E. R. 2023, *MNRAS*, 520, L38
 Donley, J. L., Brandt, W. N., Eracleous, M., & Boller, T. 2002, *AJ*, 124, 1308
 Evans, P. A., Nixon, C. J., Campana, S., et al. 2023, *NatAs*, 7, 1368
 Gafton, E., Tejada, E., Guillochon, J., Korobkin, O., & Rosswog, S. 2015, *MNRAS*, 449, 771
 Gehrels, N., Chincarini, G., Giommi, P., et al. 2004, *ApJ*, 611, 1005
 Gezari, S. 2021, *ARA&A*, 59, 21
 Golightly, E. C. A., Coughlin, E. R., & Nixon, C. J. 2019, *ApJ*, 872, 163
 Grupe, D., Beuerman, K., Mannheim, K., et al. 1995, *A&A*, 300, L21
 Guillochon, J., McCourt, M., Chen, X., Johnson, M. D., & Berger, E. 2016, *ApJ*, 822, 48
 Guillochon, J., & Ramirez-Ruiz, E. 2013, *ApJ*, 767, 25
 Guolo, M., Pasham, D. R., Zajaček, M., et al. 2024, *NatAs*, 8, 347
 Johnson, B. D., Leja, J., Conroy, C., & Speagle, J. S. 2021, *ApJS*, 254, 22

- Kara, E., Dai, L., Reynolds, C. S., & Kallman, T. 2018, *MNRAS*, 474, 3593
- Kosec, P., Pasham, D., Kara, E., & Tombesi, F. 2023, *ApJ*, 954, 170
- Lin, Z., Jiang, N., Wang, T., et al. 2024, arXiv:2405.10895
- Liu, C., Mockler, B., Ramirez-Ruiz, E., et al. 2023a, *ApJ*, 944, 184
- Liu, C., Yarza, R., & Ramirez-Ruiz, E. 2024, arXiv:2406.01670
- Liu, Z., Malyali, A., Krumpke, M., et al. 2023b, *A&A*, 669, A75
- Mainetti, D., Lupi, A., Campana, S., et al. 2017, *A&A*, 600, A124
- Manukian, H., Guillochon, J., Ramirez-Ruiz, E., & O’Leary, R. M. 2013, *ApJL*, 771, L28
- Miles, P. R., Coughlin, E. R., & Nixon, C. J. 2020, *ApJ*, 899, 36
- Nixon, C. J., & Coughlin, E. R. 2022, *ApJL*, 927, L25
- Nixon, C. J., Coughlin, E. R., & Miles, P. R. 2021, *ApJ*, 922, 168
- Pasham, D. R., & van Velzen, S. 2018, *ApJ*, 856, 1
- Pasham, D. R., Cenko, S. B., Levan, A. J., et al. 2015, *ApJ*, 805, 68
- Pasham, D. R., Lucchini, M., Laskar, T., et al. 2023, *NatAs*, 7, 88
- Payne, A. V., Shappee, B. J., Hinkle, J. T., et al. 2021, *ApJ*, 910, 125
- Payne, A. V., Shappee, B. J., Hinkle, J. T., et al. 2022, *ApJ*, 926, 142
- Payne, A. V., Auchettl, K., Shappee, B. J., et al. 2023, *ApJ*, 951, 134
- Planck Collaboration, Aghanim, N., Akrami, Y., et al. 2020, *A&A*, 641, A6
- Price, D. J., Liptai, D., Mandel, I., et al. 2024, arXiv:2404.09381
- Rees, M. J. 1988, *Natur*, 333, 523
- Sazonov, S., Gilfanov, M., Medvedev, P., et al. 2021, *MNRAS*, 508, 3820
- Schlafly, E. F., & Finkbeiner, D. P. 2011, *ApJ*, 737, 103
- Shappee, B. J., Prieto, J. L., Grupe, D., et al. 2014, *ApJ*, 788, 48
- Sironi, L., & Tran, A. 2024, *ApJ*, 968, 102
- Somalwar, J. J., Ravi, V., Yao, Y., et al. 2023, arXiv:2310.03782
- Tonry, J. L., Denneau, L., Heinze, A. N., et al. 2018, *PASP*, 130, 064505
- van Velzen, S., Farrar, G. R., Gezari, S., et al. 2011, *ApJ*, 741, 73
- Wen, S., Jonker, P. G., Levan, A. J., et al. 2024, arXiv:2405.00894
- Wevers, T., Guolo, M., Pasham, D. R., et al. 2024, *ApJ*, 963, 75
- Wevers, T., Pasham, D. R., van Velzen, S., et al. 2019, *MNRAS*, 488, 4816
- Wevers, T., Pasham, D. R., van Velzen, S., et al. 2021, *ApJ*, 912, 151
- Wevers, T., Coughlin, E. R., Pasham, D. R., et al. 2023, *ApJL*, 942, L33
- Yalinewich, A., Steinberg, E., Piran, T., & Krolik, J. H. 2019, *MNRAS*, 487, 4083
- Yao, Y., Lu, W., Harrison, F., et al. 2024, *ApJ*, 965, 39
- Yao, Y., Ravi, V., Gezari, S., et al. 2023, *ApJL*, 955, L6